Three-dimensional interpretation of electromagnetic data using a modified extended Born approximation

Hung-Wen Tseng

(formerly University of California at Berkeley,

currently Lawrence Berkeley National Laboratory)

Ki Ha Lee

(Lawrence Berkeley National Laboratory)

Alex Becker

(University of California at Berkeley)

ABSTRACT

We present a new method, dubbed the modified extended Born approximation (MEBA), for efficient three-dimensional (3-D) simulation and inversion of geophysical frequency-domain electromagnetic (EM) data for a targeted object lodged in a layered half-space. Based on the integral equation method and modified from an extended Born approximation technique, the MEBA method calculates the total electric field in an electrical conductivity inhomogeneity without any need for solving a huge matrix equation. This is done by multiplying the background electric field by a depolarization tensor. The Fourier transform and the convolution theorem are used to dramatically increase the computational efficiency. Comparisons of MEBA generated numerical data for tabular targets with data generated by other means are used to verify the scheme and check its range of validity. The results indicate that the MEBA technique yields better accuracy when current channeling in the conductivity anomaly dominates over the

induction process. The MEBA algorithm has been incorporated into a least-squares inversion scheme which is used to interpret borehole-to-surface EM tomography field data. The survey served to monitor the subsurface conductivity change associated with the extraction of a volume of saltwater previously injected into a known aquifer.

Introduction

Three-dimensional (3-D) interpretation of geophysical electromagnetic (EM) field results is very difficult because of the richness and complexity of the data and the very large number of discretized conductivity elements needed to represent a realistic geophysical model. Its success depends on the efficiency of a fast 3-D forward simulation as well as a sound inversion strategy. Complex, three-dimensional conductivity structures can be modeled using the finite element or the finite difference methods. However, the solution of the attendant huge sparse matrix equation necessary to obtain the electric and/or magnetic fields is very computationally intensive. The computational efficiency for these methods can be improved by solving the system matrix equation using massive parallel computing techniques (Alumbaugh and Newman, 1995). Unfortunately, the necessary resources for this approach are not yet generally available. Another way to model a finite inhomogeneity buried in a layered earth involves the use of the integral equation method. The advantage here is that only the solution for the electric field in the volume of interest needs to be considered. In this method (Weidelt, 1975, and Hohmann, 1975), two major steps are involved: determination of the total electric field in the confined inhomogeneity and the calculation of the scattered electric EM field at the observation locations. The latter is a

straightforward process while the former requires the solution of a Fredholm integral equation and forms a bottleneck in the computational flow.

To avoid solving the huge matrix equation one can apply a technique based on either the Born or the Rytov approximation. Both methods involve the direct replacement of the total electric fields by their background values so that matrix inversion is unnecessary. The efficiency of the algorithm is thus dramatically improved. Based on the similar approach, Zhdanov and Fang (1996) present a quasi-linear approach that now replaces the total electric field by the background field modified by a reflectivity tensor that is obtained via an optimization process.

Habashy et al. (1993) calculated the electric field inside an inhomogeneity by transforming the background electric field using a small 3x3 depolarization tensor. It is derived from the EM coupling within the anomaly itself and accounts for the depolarization effect. Their method is superior in accuracy to the Born approximation, and nearly as efficient. Based on this approximation, Torres-Verdín et al. (1994a, and 1994b) developed algorithms to image 2-D and 2-1/2D electrical anomalies and a modified version, with increased accuracy, for axial-symmetry models encountered in single-hole surveys (Torres-Verdín and Habashy, 2002). Because of its simplicity and efficiency, we have adapted this approach to develop a new EM 3-D modeling and inversion algorithm.

For 3-D forward modeling, we will use the nonlinear approximation introduced by Habashy et al. (1993), and then show how its formulation and basic assumptions must be modified to improve numerical stability of the computation. The performance of the modified nonlinear approximation technique is greatly improved by repeated application

of the Fourier transform and the convolution theorem. The forward modeling method is then incorporated into a least-squares optimization scheme for inversion of EM data. This scheme is then used to successfully recover a conductivity image from a set of borehole-to-surface (BTS) EM data acquired during an environmental remediation experiment (Tseng et al., 1998).

The modified extended Born approximation

Assuming an $e^{i\omega t}$ time dependency and following Weidelt (1975) and Hohmann (1975), for an angular frequency of ω, the electric field solution in a conductivity inhomogeneity for an electric or a magnetic source can be expressed as a Fredholm integral equation of the second kind:

$$\mathbf{E}(\mathbf{r}) = \mathbf{E}_b(\mathbf{r}) - i\omega\mu_0 \int_{V_s} \overline{\overline{\mathbf{G}}}^{E}(\mathbf{r},\mathbf{r}')\Delta\sigma(\mathbf{r}')\cdot\mathbf{E}(\mathbf{r}')d\mathbf{r}'. \qquad (1)$$

Here, $\mathbf{E}(\mathbf{r})$ and $\mathbf{E}_b(\mathbf{r})$ are respectively the total and primary electric field at a given location $\mathbf{r}$ in the anomaly and V_s is the volume which contains the confined conductivity anomalies, $\Delta\sigma$. As the frequency range used in this study does not exceed 100 kHz, the displacement current can be neglected, and the medium magnetic permeability is assumed to be that of the free space, μ_0. The Green's dyadic, $\overline{\overline{\mathbf{G}}}^{E}$, is the electric field of an electric dipole source. Once the total electric field $\mathbf{E}(\mathbf{r})$ is obtained from (1), calculation of magnetic fields at an observation location, $\mathbf{r}_r$, is straightforward using

$$\mathbf{H}(\mathbf{r}_r) = \mathbf{H}_b(\mathbf{r}_r) - i\omega\mu_0 \int_{V_s} \overline{\overline{\mathbf{G}}}^{H}(\mathbf{r}_r,\mathbf{r}')\Delta\sigma(\mathbf{r}')\cdot\mathbf{E}(\mathbf{r}')d\mathbf{r}'. \qquad (2)$$

Here, $\overline{\overline{\mathbf{G}}}^{H}$, is the Green's tensor which relates the magnetic field at the receiver location, $\mathbf{r}_r$, to the electric current element at $\mathbf{r}'$ in the inhomogeneity. Equation (1) is non-linear in the electric field $\mathbf{E(r)}$ and usually its solution is obtained numerically by dividing the anomalous region into a number of sub-domains and solving a matrix equation. This process requires a computing time that is proportional to the cube of the number of cells used to represent the anomalous body and quickly becomes impractical as the number of cells is increased. An approximate solution, using the Born approximation, can be obtained by reformulating equation (1) so that computing effort can be dramatically reduced.

Habashy et al. (1993) suggest an alternative way to linearize equation (1) by adding and subtracting, on the right-hand side, one additional term containing the total electric field $\mathbf{E}(\mathbf{r})$:

$$\begin{aligned}&\mathbf{E}(\mathbf{r}) + i\omega\mu_0\left[\int_{V_s}\overline{\overline{\mathbf{G}}}^{E}(\mathbf{r},\mathbf{r}')\Delta\sigma(\mathbf{r}')d\mathbf{r}'\right]\cdot\mathbf{E}(\mathbf{r})\\&= \mathbf{E}_b(\mathbf{r}) - i\omega\mu_0\int_{V_s}\overline{\overline{\mathbf{G}}}^{E}(\mathbf{r},\mathbf{r}')\Delta\sigma(\mathbf{r}')\cdot\left[\mathbf{E}(\mathbf{r}')\text{-}\mathbf{E}(\mathbf{r})\right]d\mathbf{r}'\end{aligned} \quad . \tag{3}$$

If the integral on the right-hand side of (3) is small compared to the background electric field $\mathbf{E}_b\mathbf{(r)}$, it can be neglected and the total electric field at any point in the inhomogeneity can be expressed as

$$\mathbf{E}(\mathbf{r}) \approx \overline{\overline{G}}(\mathbf{r})\cdot\mathbf{E}_b(\mathbf{r}), \tag{4}$$

where

$$\overline{\overline{G}}(\mathbf{r}) = \left[\overline{\overline{\mathbf{I}}} + iwm_0\int_{V_s}\overline{\overline{\mathbf{G}}}^{E}(\mathbf{r},\mathbf{r}')\Delta s(\mathbf{r}')d\mathbf{r}'\right]^{-1}. \tag{5}$$

The 3x3 dyadic $\overline{\overline{G}}$ in (5) is the depolarization tensor introduced by Habashy et al. (1993). It has a DC limit which accounts for the difference in amplitude between the total internal electric field and the background field caused by charge accumulations on the boundaries of the inhomogeneity. This approximation is equivalent to assuming that the electric field at any point in the region of the inhomogeneity, $\mathbf{r}'$, is equal to the value at the location $\mathbf{r}$ for which it is being calculated. The dominant contribution to the second integral in (3) comes from points in the vicinity of $\mathbf{r}$ due to the locally singular nature of $\overline{\overline{\mathbf{G}}}^{E}(\mathbf{r},\mathbf{r}')$ at $\mathbf{r}'=\mathbf{r}$. As a result, the approximation is appropriate as long as the internal electric field is a smoothly varying function of position so that the local difference in the electric field, $\mathbf{E}(\mathbf{r}')-\mathbf{E}(\mathbf{r})$, is small when $\mathbf{r}'$ approaches $\mathbf{r}$.

Habashy et al. (1993) have demonstrated that, for a sphere of uniform conductivity located in a homogeneous conductive whole space, this approximation is more accurate than the Born approximation where larger electrical structures, a larger conductivity contrast between the anomaly and the background host, and a wider frequency range are involved. However, one can reasonably expect that this approximation is likely to be inaccurate at locations that are close to a source or the conductivity interface in an anomalous region. Torres-Verdíne and Habashy (2002) introduced a correction term to evade the source proximity problem for axially-symmetric models in a whole space but did so at the cost of computing efficiency. This technique is called the localized nonlinear approximation by Habashy et al. (1993) and the extended Born approximation (EBA) by Torres-Verdín (1994a). The latter terminology will be followed in this study because it is indicative of this technique's relationship to the Born approximation.

A major advantage of this approximation technique is that it is as efficient as the Born approximation but only requires the solution of a 3x3 matrix for the depolarization tensor in each discretized cell to obtain the total electric field. Additionally, the depolarization tensor in (5) is not related to the source type or source location but only depends on the geometry of the inhomogeneity and the wave propagation constant of the medium. This makes the technique very appealing for computations involving multiple sources.

A closer investigation of the EBA approach, however, reveals a numerical instability problem when the conductivity in the anomalous volume is discontinuous. This can be seen considering a sketch of a discretized conductivity anomaly, shown in Figure 1, which consists of only two cubic cells located in a 0.1 S/m whole space. If the anomalous conductivity of cell one, $\Delta\sigma_1$, is 0.2 S/m while that of cell two, $\Delta\sigma_2$, is 1.23 S/m, the real part of the tensor computed from the integral of (5) for cell one, at 100 Hz (with the imaginary part neglected), is approximately

$$\begin{bmatrix} -1 & 0 & 0 \\ 0 & 1.5 & 0 \\ 0 & 0 & 1.5 \end{bmatrix}.$$

The calculation of (5) involving integration over the source region was carried out based on Chew (1989). The tensor element Γ_{xx} for cell number one is therefore almost singular and it maps the background electric field, $E_{b,x}$, near infinity. This cannot be physically correct, and results in erroneous electric field values in the conductivity inhomogeneity. In other words, when the conductivity gradient of the inhomogeneity is parallel to any component of the background electric field, the EBA approximation may fail. This is a critical factor for inversion methods based on this forward calculation since the inverted

domain is usually inhomogeneous in conductivity. From a physical perspective, the failure is caused by the assumption that the electric field is constant over the entire conductivity anomalous region. However, this cannot be true if the conductivity distribution in the inhomogeneity is discontinuous. The physical parameter that is continuous across the conductivity boundary is the normal electric current density, which is the product of the conductivity and the total normal electric field.

To improve the numerical reliability for EBA, we replace the added $\mathbf{E}(\mathbf{r})$ term in (3) with $\sigma(\mathbf{r})/\sigma(\mathbf{r}')\cdot\mathbf{E}(\mathbf{r})$ and obtain the following form that evades the singularity problem:

$$\begin{aligned}&\mathbf{E}(\mathbf{r})+iwm_0\left[\int_{V_s}\overline{\overline{\mathbf{G}}}^{E}(\mathbf{r},\mathbf{r}')\Delta s(\mathbf{r}')\frac{s(\mathbf{r})}{s(\mathbf{r}')}d\mathbf{r}'\right]\cdot\mathbf{E}(\mathbf{r})\\&=\mathbf{E}_b(\mathbf{r})-iwm_0\int_{V_s}\overline{\overline{\mathbf{G}}}^{E}(\mathbf{r},\mathbf{r}')\frac{\Delta s(\mathbf{r}')}{s(\mathbf{r}')}\left[s(\mathbf{r}')\cdot\mathbf{E}(\mathbf{r}')-s(\mathbf{r})\cdot\mathbf{E}(\mathbf{r})\right]d\mathbf{r}'\end{aligned}. \qquad (6)$$

Again, if the second integral on the right side of (6) is negligible compared to the background electric field, the total electric field in the anomalous region now can be approximated by

$$\mathbf{E}(\mathbf{r})\approx\overline{\overline{\mathrm{G}}}^{m}(\mathbf{r})\cdot\mathbf{E}_b(\mathbf{r}), \qquad (7)$$

where

$$\overline{\overline{\mathrm{G}}}^{m}(\mathbf{r})=\left[\overline{\overline{\mathbf{I}}}+iwm_0 s(\mathbf{r})\int_{V_s}\overline{\overline{\mathbf{G}}}^{E}(\mathbf{r},\mathbf{r}')\frac{\Delta s(\mathbf{r}')}{s(\mathbf{r}')}d\mathbf{r}'\right]^{-1}. \qquad (8)$$

The superscript *m* attached to the two tensors in (7) and (8) indicates that they are 'modified' from the extended Born approximation to form the MEBA. The electric current density within the inhomogeneity must vary smoothly to ensure the quality of the approximation. If the conductivity in the anomalous region is uniform, the tensor, $\overline{\overline{\mathrm{G}}}^{m}$, in

(8) is the same as the tensor $\overline{\overline{G}}$ in (5). Though the MEBA stabilizes the extended Born approximation numerically, the assumption of the constant electric current density forces the electric field tangential to the conductivity variation boundary to be discontinuous, which is also physically incorrect. For example, if σ_2 in Figure 1 is changed to 0.01, Γ_{yy} is close to –1 and (7) will fail as well. However, the contrast between σ_1 and σ_2 now is as large as 120 and this can be controlled by smoothing the conductivity in the inverted domain.

Use of the Fourier transform

A further study of the modified extended Born approximation (MEBA) exposes two problems that limit its practicality for three-dimensional EM modeling as the number of the discrete cells increases. First, the computing time increases at a rate proportional to the square of the number of the discretized cells. Also, the memory required for storing the Green's dyadic used in (8) increases dramatically. These difficulties can be overcome by identifying the MEBA integrals in (8) as convolutions of the Green's dyadic and the normalized anomalous conductivity, and applying the Fourier transform to them (Tseng et al., 1996). A similar approach has been used in the work of Lajoie (1975) to obtain the EM response of an arbitrary source on a layered earth.

Rearrange the integral of (8) and one obtains

$$\overline{\overline{G}}^{m}(x,y,z)=\left[\overline{\mathbf{I}}+iwm_0 s(x,y,z)\cdot \mathrm{IFT}_{(k_x k_y)}\left\{\int_{z'}\tilde{\overline{\overline{\mathbf{G}}}}^{\mathrm{E}}(k_x,k_y,z)\tilde{\mathrm{Q}}(k_x,k_y,z')dz'\right\}\right]^{-1}. \qquad (9)$$

Here, k_x and k_y are the spatial wavenumbers for the X- and Y-coordinates, respectively; $\mathrm{IFT}_{(k_x,k_y)}$ stands for the two-dimensional inverse Fourier transform applied to the result of the integration in the bracket; and $\overline{\overline{\mathbf{G}}}^{\mathrm{E}}$ and $\tilde{\mathrm{Q}}$ are the wavenumber counterpart of $\overline{\overline{\mathbf{G}}}^{\mathrm{E}}$ and the normalized conductivity anomaly, $\Delta\sigma(x',y',z')/\sigma(x',y',z')$, respectively. The convolution is not applied in the vertical Z-coordinate because the Green's dyadic is not invariant in this dimension for a layered half space. Since the calculation of the scattered magnetic fields at the receiver locations is also a convolution of the Green's function and the electric current density, convolution theory also applies as well.

With the FFT technique, the computing time is now proportional to $(N_x \log_2 N_x)(N_y \log_2 N_y)N_z^2$, where N_x, N_y, and N_z are the numbers of samples used to represent the 3-D model. In addition, Green's functions in a whole space or in a horizontally layered host medium have a closed form in the wavenumber domain (Ward and Hohmann, 1987). This results in a significant reduction in the amount of memory required and associated I/O activity during the calculation.

Extra care must be exercised to allow for the behavior of the Green's function in its closed form as it is not band-limited and does not have a Nyquist frequency in the (k_x, k_y, z) domain. As a result, a low-pass Blackman-Harris filter (Harris, 1978) is applied to the transformed conductivity anomaly to eliminate any aliasing error.

Accuracy of the MEBA method

To assess the accuracy of the MEBA technique in typical working conditions, the MEBA simulation results for a borehole-to-surface survey over a plate-like model are compared with those derived with the 3-D integral equation method (Wannamaker, 1984).

As shown in Figure 2(a), a horizontal 13x13x1 m thin plate is placed at a depth of 30 m in a homogeneous 0.1 S/m half-space. Its conductivity, as presented in Figure 2(b), varies linearly from 0.33 S/m at the edges to 1 S/m at the center. A vertical magnetic dipole source operating at a frequency of 10 kHz is located at the level of the conductive plate. Nineteen magnetic field sensors are deployed along a surface profile at 5 m intervals, for a distance of 45 m on either side of the transmitter borehole. The total electric field amplitudes on the thin body in the Y-direction, E_y, computed with the three methods: 3-D integral equation method (EM3D), MEBA, and EBA, are shown for comparison in Figures 2(c), (e), and (g), respectively. The corresponding differences in E_y with respect to the results derived with EM3D are presented in Figures 2(d) and (f), respectively. At internal locations all three numerical codes yield similar results. However, at the plate edges normal to the primary dominant E-field, the electric field obtained with the MEBA is off by about 30%, while the EBA results are about twice as large as those computed with the integral equation method. A comparison of the corresponding vertical and horizontal components of the scattered magnetic fields at the surface receiver positions at 10 kHz is shown in Figure 3. With the MEBA technique, the normalized rms error in amplitude is about 3.5% while it is 12% for the EBA technique.

The corresponding rms errors in phase are 0.6 and 1.2 degrees, respectively, for the two methods.

Range of validity for the MEBA

As indicated by Walker and West (1992) for a conductive host medium, galvanic current (or current channeling) as well as inductive current in the target contributes to the observed fields. The latter is a vortex current that is located within the conductivity anomaly, while the former flows through the anomaly-host boundary. This raises the possibility that the MEBA method may be more accurate when used in situations where current channeling is dominant than in those where EM induction prevails. Since the bounded induced electric current flows in a circular pattern, it violates the constant current density assumption. To verify this hypothesis and to examine the relationship between the range of validity for the MEBA technique and the relative importance of the two current modes in an EM scattering problem, we examine the MEBA results for two thin plate models, one with a current-channeling dominance and the other with strong induction.

Based on Walker and West (1992), the relative significance of the current channeling to the induction effect can be described by a dimensionless current-excitation ratio (CER). If the CER value is greater than one, the galvanic effect dominates induction, and vice versa. Since the CER value for any given model depends on host conductivity, target conductance, frequency, the geometry of the model, and its position relative to the exciting source, it should prove to be a useful tool for evaluating the

accuracy of the MEBA method. In general, CER values in a closed form are not available. Consequently, we have calculated the CER values for the chosen model using program SHEETS (Zhou, 1989) where the total electric surface current density on the thin sheet can be decomposed into its galvanic and the inductive components. The CER number is obtained by dividing the rms value of the galvanic current density on the plate by that caused by induction.

The calculations were done for the model sketched in Figure 2(a) for a frequency range of 100 Hz to 100 kHz. While the host conductivity being held constant, the conductivity contrasts between the anomalous body and the background medium changes by factors ranging between 2.5 to 40 in steps of 2.5. The relative difference between the MEBA data and the EM3D results for the vertical magnetic fields at surface as a function of frequency and conductivity contrast and its relationship to the corresponding CER numbers are shown in the form of faceted contour plots in Figures 4(a) and (b), respectively. Clearly, for this specific model, the normalized rms MEBA errors are smaller at lower frequencies and for lower conductivity contrasts. An inverse correlation is observed between the MEBA errors and the CER values: the larger the latter, the smaller the error.

An extreme case where the inductive effect dominates the current channeling can be obtained by placing the center of the plate at the borehole and by positioning the source 15 m below it. Again, the normalized rms MEBA errors in the vertical magnetic field resulting from the MEBA and the corresponding CER values are displayed in Figures 5(a) and (b), respectively. All the CER values for this model are smaller than 0.3, indicating that the induction is much stronger than the current channeling and rms

errors are more than twice as big as that of the previous model. However, for conductivity contrasts smaller than five and frequencies lower than 10 kHz, the errors do not exceed 10%.

Three-dimensional Inversion using the modified extended Born approximation

An efficient iterative 3-D EM inversion algorithm based on the least-squares criteria has three features: a fast forward simulation algorithm for calculating the EM system response to a conductivity distribution; an effective method of calculating the Jacobian matrix which relates the calculated EM fields to any perturbation of the conductivity model; and an effective scheme to solve the large, ill-posed, system matrix equation for the updated conductivity structure. The MEBA technique easily meets the first two requirements.

The goal of automatic interpretation is to find a discretized model, defined by its parameter vector $\mathbf{m} = (\mathrm{m}_1, \mathrm{m}_2, \ldots, \mathrm{m}_M)^T$ (in this case the subsurface conductivity distribution), that can fit the magnetic field data, d^{obs}, as closely as possible. Here, *M* denotes the total number of discretized cells composing the conductivity distribution, N is the number of observed data and *T* denotes the transpose of the matrix. Following Oldenburg et al. (1993), the desired model, m^{k+1}, is derived by iteratively solving the following system matrix equation:

$$(\bar{\bar{\mathbf{J}}}^T \bar{\bar{\mathbf{W}}}_d^T \bar{\bar{\mathbf{W}}}_d \bar{\bar{\mathbf{J}}} + \lambda \bar{\bar{\mathbf{W}}}_m^T \bar{\bar{\mathbf{W}}}_m)\mathbf{m}^{k+1} = \bar{\bar{\mathbf{J}}}^T \bar{\bar{\mathbf{W}}}_d^T \bar{\bar{\mathbf{W}}}_d (\bar{\bar{\mathbf{J}}}\mathbf{m}^k - \mathbf{d}(\mathbf{m}^k) + \mathbf{d}^{obs}). \qquad (10)$$

Here, *k* is the iteration number and $\mathbf{d}(\mathbf{m})$ is a one-dimensional vector representing the calculated system response to the associated subsurface conductivity model, $\mathbf{m}^k$; $\bar{\bar{\mathbf{W}}}_d$ is a

$N \times N$ weighting matrix that assigns a relative importance to each data point. The two-dimensional $M \times M$ weighting matrix, $\overline{\overline{\mathbf{W}}}_m$, determines how the model is biased. In this study, smoothness is used as the criterion and is defined as the first spatial derivative of the conductivity in all three coordinates. The variable λ in (10) is a Lagrange multiplier that controls the degree of smoothness of the model. Following Newman and Alumbaugh (1996), its initial value is determined by an estimate of the largest eigen-value of the non-regularized least-squares system matrix. If the updated conductivity structure reduces the data misfit, the Lagrange multiplier is reduced by half to allow for a rougher conductivity structure.

Based on (2), the Jacobian matrix, $\overline{\overline{\mathbf{J}}}$, which is the change in the EM field for each source-receiver pair due to the perturbation of each element of the discretized conductivity model, is expressed as

$$\frac{\delta \mathbf{H}(\mathbf{r}_r)}{\delta \sigma} = -i\omega\mu_0 \int_{V_s} \overline{\overline{\mathbf{G}}}^{H}(\mathbf{r}_r, \mathbf{r}) \cdot \mathbf{E}(\mathbf{r}) d\mathbf{r}, \qquad (11)$$

where $\mathbf{E(r)}$ is the total electric field in the inhomogeneity due to the transmitter source and $\mathbf{r}_r$ is the receiver position. Following Brian & Habashy (1995), $\overline{\overline{\mathbf{G}}}^{H}(\mathbf{r}_r, \mathbf{r})$ in (11) may be replaced by the electric field due to a fictitious magnetic dipole source at the receiver location and is polarized in the direction of the observed magnetic field. As a result, the element of the Jacobian matrix, the *i*-th source-receiver pair due to the conductivity perturbation of the *j*-th cell, can now be rewritten as

$$\mathbf{J}_{ij} = -i\omega\mu_0 \int_{V_j} \mathbf{E}_j^*(\mathbf{r}) \cdot \mathbf{E}_j(\mathbf{r}) d\mathbf{r},$$

where $\mathbf{E}_j(\mathbf{r})$ is the total electric field in the j-th cell due to the transmitter source, and $\mathbf{E}^*_j(\mathbf{r})$ is the electric field, also in the j-cell, due to the fictitious unit moment magnetic dipole. Since the electric field is assumed constant over the discretized cell, the Jacobian is approximated by:

$$\mathbf{J}_{ij} \approx -iw\mu_0 \left(\overline{\overline{\mathbf{G}}}^m_j \cdot \mathbf{E}^*_{\mathrm{b},j} \right) \cdot \left(\overline{\overline{\mathbf{G}}}^m_j \cdot \mathbf{E}_{\mathrm{b},j} \right) \Delta \mathrm{V}_j \, .$$

Here, $\Delta \mathrm{V}_j$ is the volume of the cell, and $\mathbf{E}_{\mathrm{b},j}$ and $\mathbf{E}^*_{b,j}$ are the background electric fields in the inhomogeneity due to the two transmitter sources, respectively. Taking advantage of the fact that background electric fields, $\mathbf{E}_\mathrm{b}$ and $\mathbf{E}^*_\mathrm{b}$, are invariant throughout the inversion process and that the depolarization tensors have been derived in the previous forward simulation, the approximate Jacobian matrix can be efficiently evaluated.

Inversion of simulated data

To test the newly developed 3-D inversion code, we use a set of borehole-to-surface (BTS) numerical simulation data. The simulated model and the corresponding data are the same as those used to interpreted the results of a BTS experiment previously described by Tseng et al. (1998). Here, as sketched in Figure 6, two 0.2 S/m horizontal thin sheets are located at depths of 26 and 30 m, respectively, in a 0.1 S/m homogeneous half space. The top conductor has a dimension of 6x4x2 m and the lower one, 12x10x3 m. Both plates are intersected by a transmitter well at 1.3 and 2.5 m, respectively, from their centers. The direction of their longer axis deviates from the X-coordinate axis by 30 degrees. In this BTS configuration, the transmitter traverses the vertical borehole from a

depth of 60 m up to 15 m with stations at 2.5 m intervals. The receivers are deployed at 5 m along two orthogonal surface profiles centered on the top of the transmitter borehole. Total vertical magnetic fields calculated with the thin sheet code (Zhou, 1989) along the two surface profiles are used as input data for the newly developed inversion algorithm. The numerical simulation data were degraded to an accuracy of 1% amplitude and 1° phase noise by the addition of random noise. The inversion domain, with its surface projection centered at the transmitter well, is a 42x42x30 m volume discretized into 21x21x15 cubic cells and located in depth between 5 m and 35 m levels.

The inverted conductivity distribution, based on data from both surface profiles, is shown in Figure 7(a). The projections of the anomalous bodies in the vertical plane, which contains the surface X-profile and the transmitter borehole, and on the horizontal slice at 28 m depth are outlined for comparison with the MEBA based data inversion. The depth of the anomalous zone is recovered, so are the orientations of the two plates. However, the interpretation results fail to show the vertical separation between the two plates. This is due to the smoothness constraint applied to the inversion process and non-uniqueness inherent in the inversion. Another problem that should be considered in a 3-D interpretation is the spatial coverage of the survey. If it is insufficient, the resulting inversion results may be incorrect. For example, Figure 7(b) shows the inverted image derived only from the surface X-profile data only. While the depth of the anomalous zone is recovered, the orientation of the two plates is incorrect.

Three-dimensional inversion of the Richmond Borehole-to-surface EM data

We have attempted to invert a set of 10 kHz BTS EM field data acquired at the University of California Richmond Field Station, where a brine spill was simulated by creating a saline water injection zone at a depth of about 30 m. The plume, whose extent was to be determined from the post-injection BTS data, was later extracted and the experiment was construed as a means for validating a remediation process. The test site and the field layout, along with the surface projection of the previously interpreted saltwater plume, are sketched in Figure 8. Details relevant to the experiment, the geology of the test site, the instrumentation, the acquired data, as well as its interpretation by trial-and-error, are described in Tseng et al. (1998). The vertical component of the magnetic fields was sampled at 4 m intervals along two surface profiles, labeled as NW-SE and the SW-NE profiles in Figure 8. The SW-NE profile was so seriously contaminated by the presence of some very shallow metal debris so that only the data for the NW-SE profile are useful for inversion. This profile is centered on the injection well INJ1 and runs for 44 m in either direction. Measurements could not be made at the wellhead station. Nineteen transmitter positions, at 2.5 m intervals, were located in INJ1 between the 15 m to 60m depth levels. The inversion domain, based on a 4 m cube grid, is an 88x88x64 m volume with its surface projection centered on the injection well INJ1, and a vertical extent from 2 to 66 m depth. Both data sets, acquired before and after the water extraction, were inverted using a 12 ohm-m homogeneous half space as the initial model.

Figure 9(a) illustrates the pre-extraction magnetic field amplitudes, in units of dB above 1 nA/m, along the surface profile in the form of a contoured section where each

datum position is defined by a transmitter depth and surface receiver station position. The data misfits of the inversion results relative to the measured data are also displayed in Figure 9(b). A vertical section containing the NW-SE profile, and a horizontal slice, at 28 m depth, of the pre-extraction conductivity distribution obtained from the inversion procedure are shown in Figure 10(a). The corresponding post-extraction results are displayed in Figure 10(b). The two distinct units with a boundary at about 40 m depth correspond respectively to the already known sediments and the basement at the test site. The injected saltwater plume manifests itself as a small conductive region, absent in the post-extraction results shown in Figure 10(b), of about 0.12 S/m located next to the injection well at 30 m depth. The conductivity change due to the water removal is expressed in Figure 10(c) in percentage terms relative to the conductivity before the pumping. Clearly, the effect of the pumping has reduced the conductivity of the injected zone by as much as 35%. Due to the poor quality of the other surface profile, there is not enough spatial coverage to define properly the conductivity change in that lateral direction. However, the pre-extraction inversion results do indicate that the distribution of the saltwater was asymmetric about the transmitter well with its center shifted to the northwest of the injection well.

Discussion

Based on the assumption that the electric current density is constant within the anomalous region as the EM coupling between any two points in the inhomogeneity is calculated, the MEBA technique improves the numerical validity of the extended Born approximation. However, like the Born approximation, the MEBA method tends to be

more accurate for low frequencies and at low conductivity contrasts. More specifically, its accuracy depends on the relative dominance of the galvanic and the induction effects in the scatterer. The stronger the current channeling, the better the simulation results. The utility of the MEBA technique is much improved with the use of the Fourier transform and convolution theory. Convolution of the Green's function and the normalized conductivity anomaly (or the current density) in the wavenumber domain makes the computation much more efficient.

When incorporated into a least-squares optimization process, the MEBA method offers a remarkably efficient way to compute the Jacobian matrix for updating the conductivity structure. With proper space coverage the inversion results for the simulation data show successful recovery of the 3-D conductivity anomaly. The interpreted results of the BTS field experiment, even with data along just one surface profile, are consistent with those obtained by a trial-and-error fit to the field data. However, solving the system matrix equation in the inversion requires more than 90% of the memory and 95% of the computing time. This arises because of the memory needed to store the Jacobian matrix and the results of the multiplication with its own transpose, while most of the computing time is spent to invert the matrix equation for updating the conductivity structure. Consequently, the model size is limited and depends on the available system resources. An improved performance strategy for the inversion is under development.

Acknowledgements

This work was supported by the Office of Basic Energy Sciences, Engineering and Geosciences Division, and by the Assistant Secretary for Fossil Energy, Office of Gas and Petroleum Technologies, of the U.S. Department of Energy under Contract No. DE-AC03-76SF00098. We thank Professor Frank Morrison for his many constructive comments.

References

Alumbaugh, D. L., and Newman, G. A., 1995, Time efficient 3-D electromagnetic modeling on massively parallel computers: Intern. Symp. on Three-Dimensional Electromagnetics, Ridgefield, Connecticut, U.S.A., 205-218.

Chew, W. C., 1989, Some observations on the spatial and eigenfunction representations of dyadic Green's functions: IEEE Trans. Antennas Propagat., **37**, 1322-1327.

Habashy T. M., Groom, R. W., and Spies, B., 1993, Beyond the Born and Rytov Approximations: A nonlinear approach to electromagnetic scattering: J. Geophys. Research, **98**, 1759-1775.

Harris, F., 1978, On the use of windows for harmonic analysis with the discrete Fourier transform: Proceedings of the IEEE, **66**, 51-83.

Hohmann, G. W., 1975, Three-dimensional induced polarization and electromagnetic modeling: Geophysics, **40**, 309-324.

Lajoie, J. L., 1975, EM response of an arbitrary source on a layered earth: a new computational approach: Geophysics, 40, 773-789.

Newman, G., and Alumbaugh, D. L., 1996, Three-dimensional electromagnetic modeling and inversion on massively parallel computers: Sandia National Labtoratories Report SAND96-0582.

Oldenburg, D. W., McGillivray, P. R., and Ellis, R. G., 1993, Generalized subspace methods for large-scale inverse problems: Geophys. J. Int., **114**, 12-20.

Spies, B. R. and Habashy, T. M., 1995, Sensitivity analysis of crosswell electromagnetics: Geophysics, **60,** 834-845.

Torres-Verdín, C., and Habashy, T. M., 2002, Rapid numerical simulation of axisymmetric single-well induction data using the extended Born approsimation: Radio Science, **36**, 1287-1306.

Torres-Verdín, C., and Habashy, T. M., 1994a, A two-step linear inversion of two-dimensional electrical conductivity: SPIE, v. 2241, Inverse Optics III, 40-54.

Torres-Verdín, C., and Habashy, T. M., 1994b, Rapid 2.5-D forward modeling and inversion via a new nonlinear scattering approximation: Radio Science, **29**, 1051-1079.

Tseng, H.-W., Becker, A., Wilt, M., and Deszcz-Pan, M., 1998, A borehole-to-surface electromagnetic survey: Geophysics, **63**, 1565-1572.

Tseng, H. -W., Becker, A. and Lee, K. H., 1996, An improved numerical technique for 3-D electromagnetic modeling, 66th Ann. Internat. Mtg: Soc. of Expl. Geophys., 249-252.

Walker, P. W., and West, G. F., 1992, Parametric estimators for current excitation on a thin plate: Geophysics, **57**, 766-773.

Wannamaker, P. E., Hohmann, G. W., and San Filipo, W. A., 1984, Electromagnetic modeling of three-dimensional bodies in layered earths using integral equations: Geophysics, **49**, 60-74.

Ward, S. H., and Hohmann, G. W., 1987, Electromagnetic theory for geophysical applications: *in* M. N. Nabighian, ed., Electromagnetic Methods in Applied Geophysics --- Theory, v.1, Soc. Explor. Geophys., 131-311.

Weidelt, P., 1975, Electromagnetic induction in three-dimensional structures: J. Geophys., **41**, 85-109.

Zhdanov, M. S., and Fang, S., 1996, Quasi-linear approximation in 3-D electromagnetic modeling: Geophysics, **61**, 646-665.

Zhou, Q., 1989, Audio-frequency electromagnetic tomography for reservoir evaluation: Ph.D. thesis, Univ. of California at Berkeley.

Figure captions

Fig. 1 A simplified model to demonstrate existence of a possible singularity in the depolarization tensor.

Fig. 2 Comparisons of simulation results computed with the integral equation method (EM3D), the modified Born approximation (MEBA), and the extended Born approximation (EBA), respectively; (a) Model geometry; (b) plan view of the conductivity distribution in the anomaly; (c), (e), and (f) are contoured Y-component total electric field in the anomaly derived with the three methods; (d) and (f) are the relative difference in E_y derived from MEBA and EBA, respectively, with respect to EM3D.

Fig. 3 Comparisons of horizontal and vertical magnetic secondary fields calculated with the three numerical methods at surface receiver locations as sketched in Figure 2(a).

Fig. 4 Faceted contour plots of (a) rms error in the vertical magnetic field component, and (b) corresponding CER values as a function of conductivity contrast and frequency for the galvanic effect dominance model.

Fig. 5 Faceted contour plots of (a) rms error in the vertical magnetic field component, and (b) corresponding CER values as a function of conductivity contrast and frequency for the model with strong induction.

Fig. 6 A two-sheet model used to produce simulation data for testing the 3-D inversion code.

Fig. 7 Inversion results using (a) both surface profiles, and (b) the X-profile only.

Fig. 8 Field map of the Richmond Field Station test site (after Tseng et al., 1998).

Fig. 9 (a) Measured pre-extraction vertical magnetic field amplitudes expressed in units of dB above 1 nA/m. (b) Data misfits of the inversion results with respect to the measured pre-extraction field data.

Fig. 10 Three-dimensional MEBA inversion results using (a) pre-extraction BTS data and (b) post-extraction data. The vertical section contains the transmitter well and the surface profile while the horizontal slice is at the depth of 28 m. (c) Conductivity change, in percentage with respect to the pre-extraction conductivity.

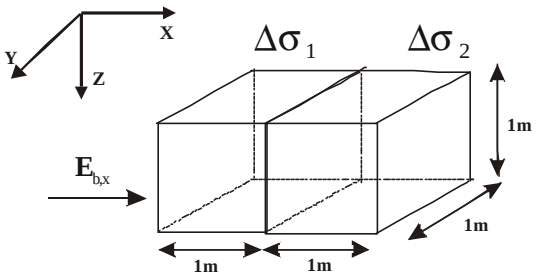

Tseng et al., Fig. 1, column width.

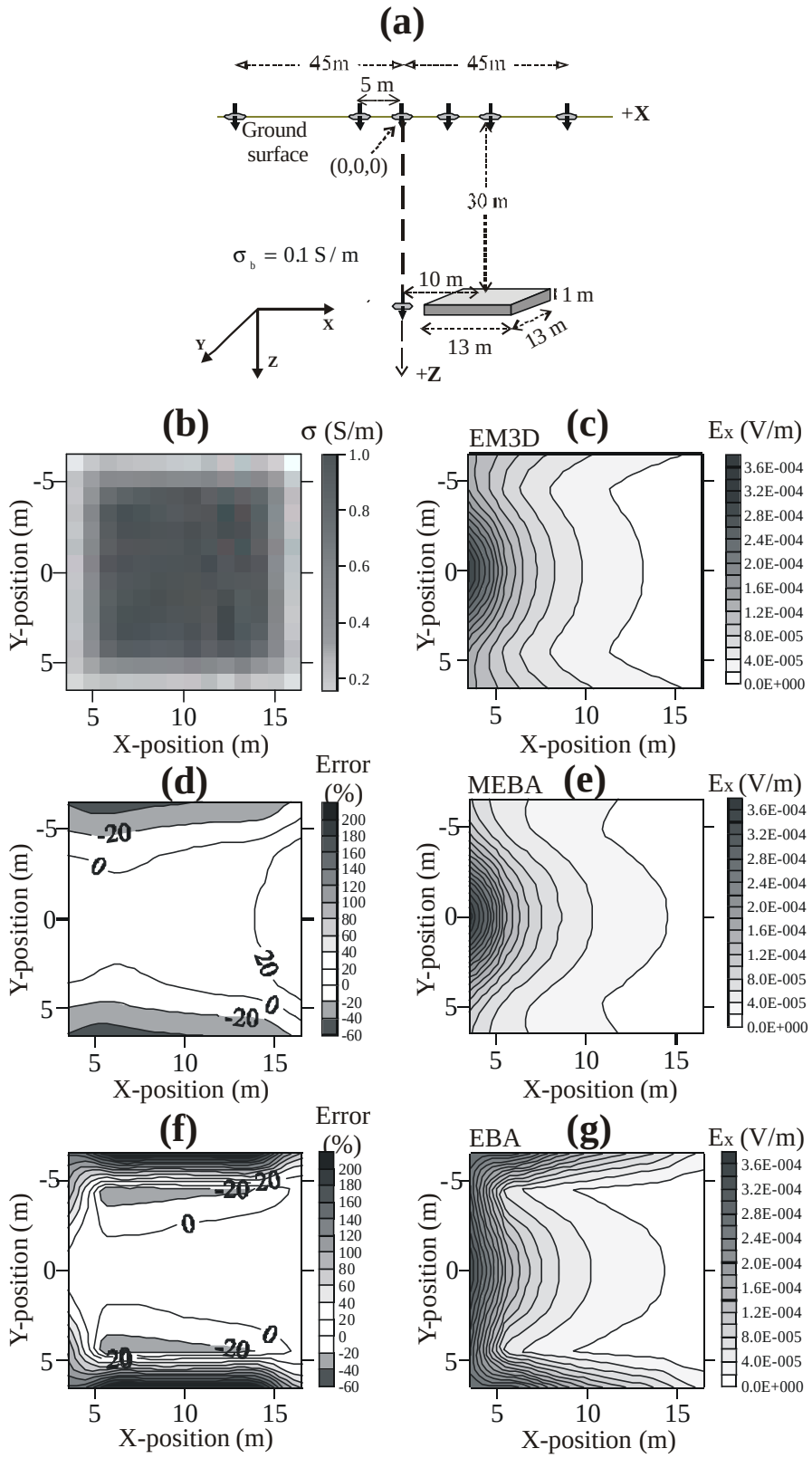

Tseng et al., Fig. 2, page width

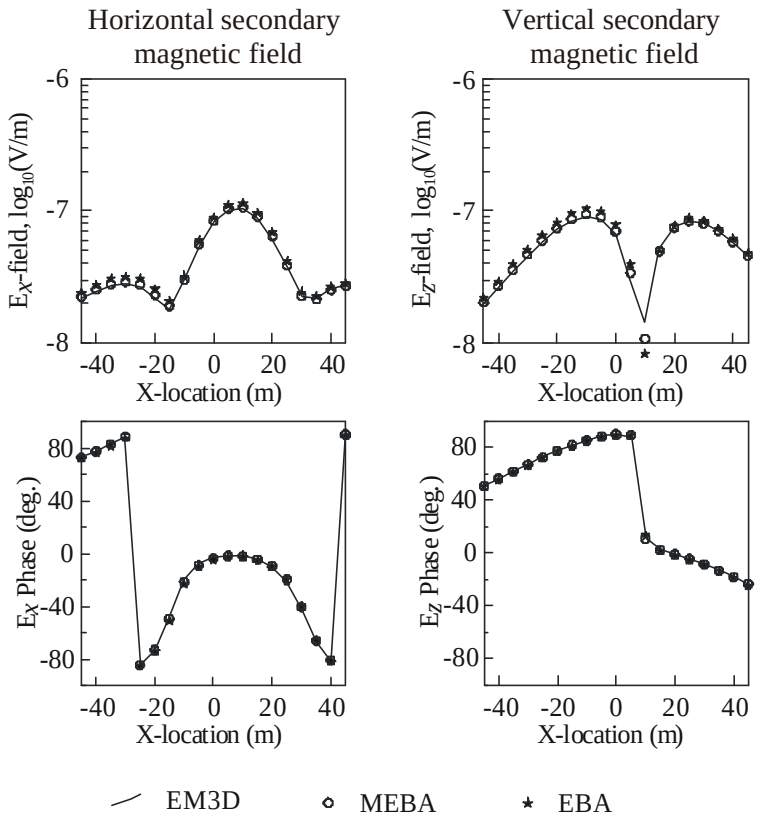

Tseng et al., Fig. 3, page width.

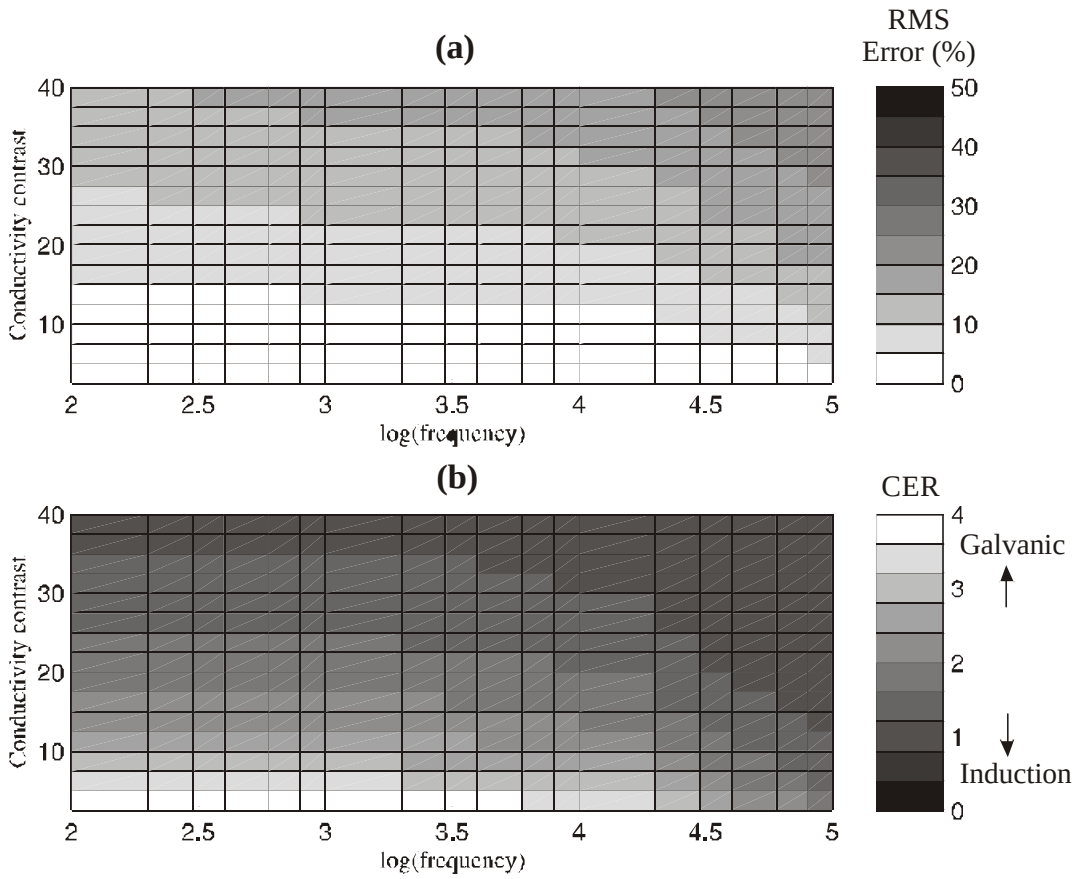

Tseng et al., Fig. 4, page width.

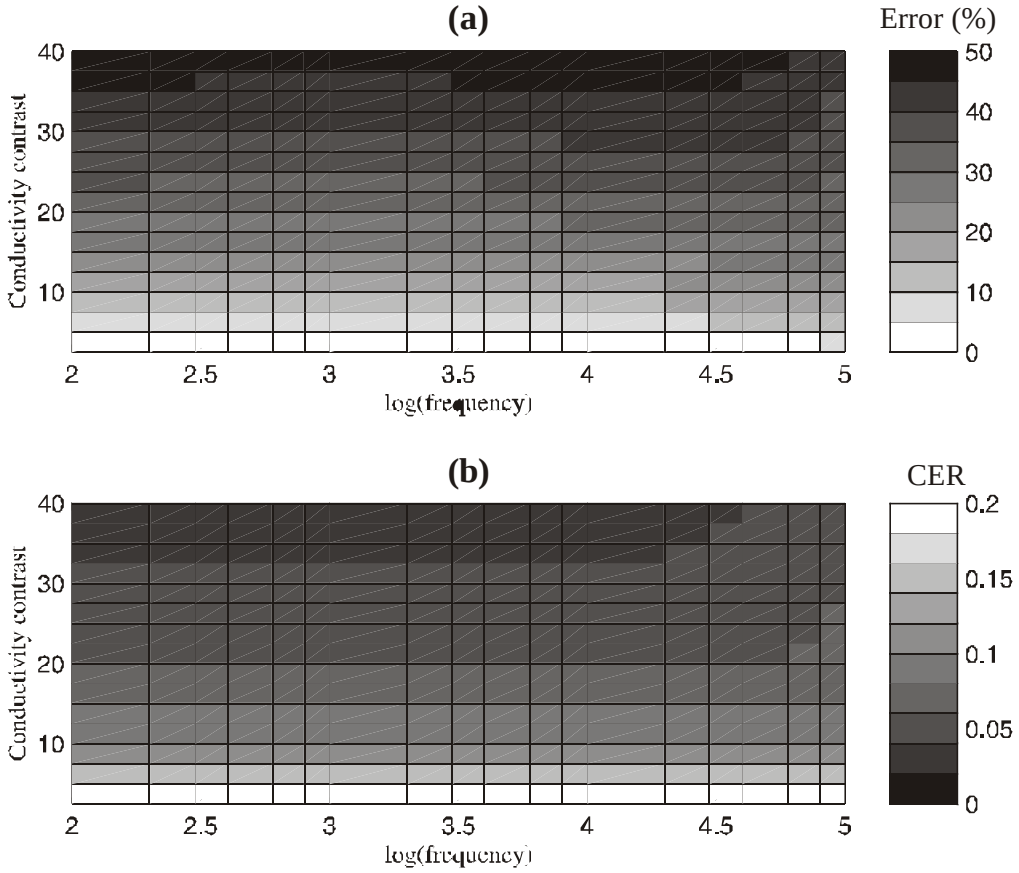

Tseng et al., Fig. 5, page width.

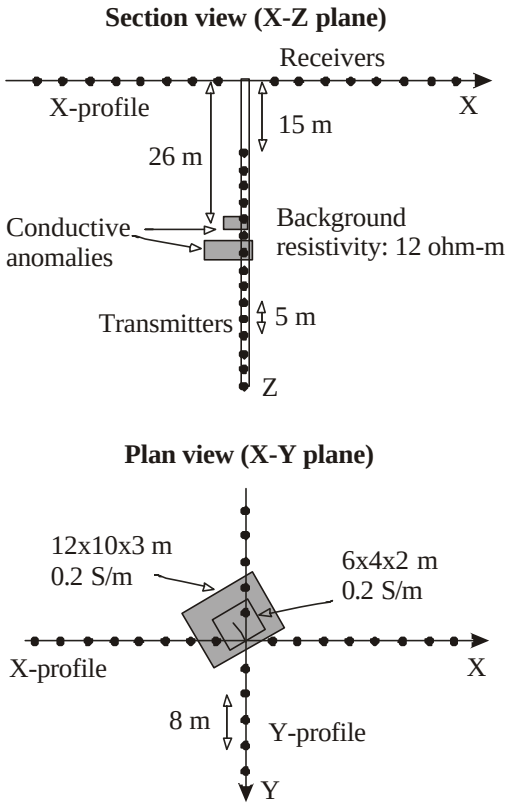

Tseng et al., Fig. 6, column width.

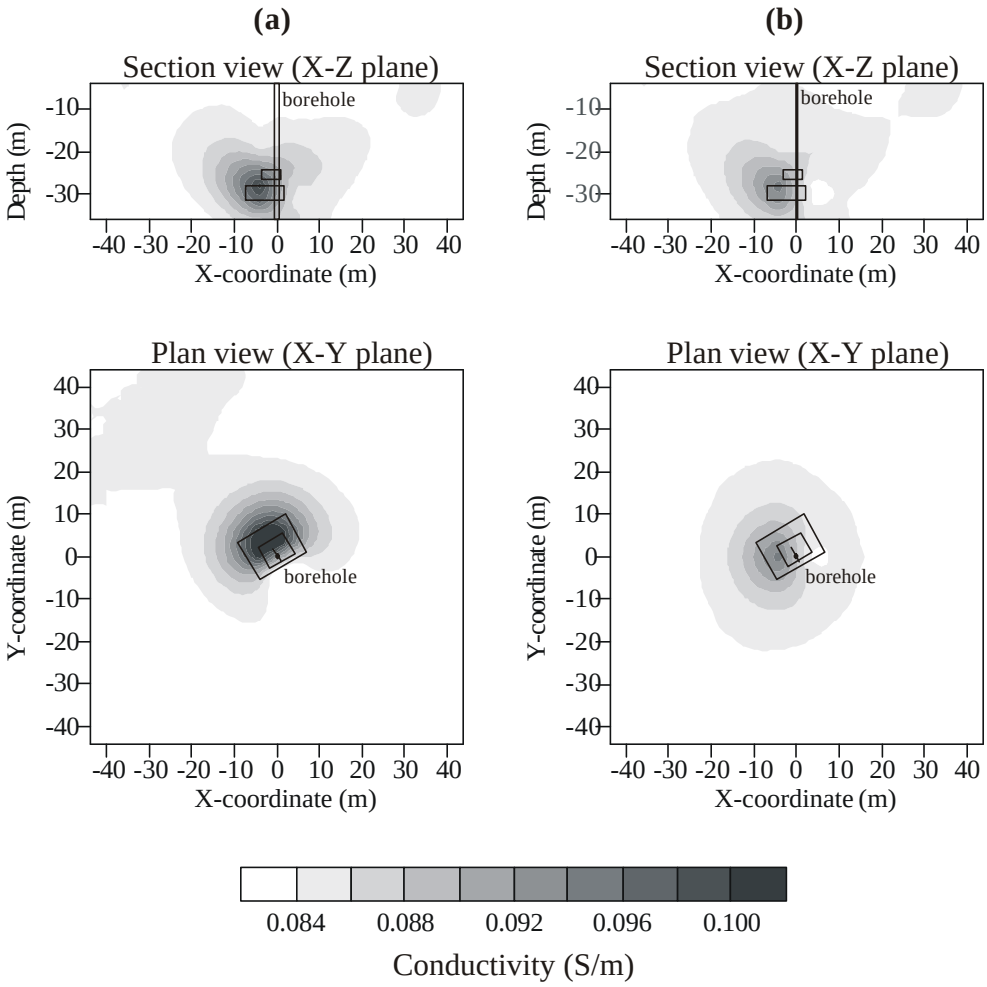

Tseng et al., Fig. 7, page width.

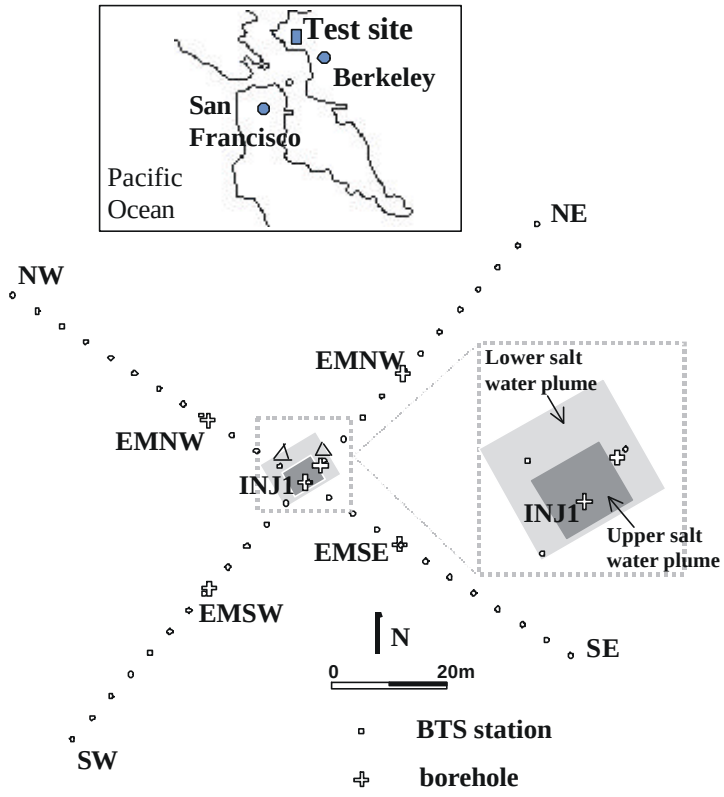

Tseng et al., Fig. 8, page width.

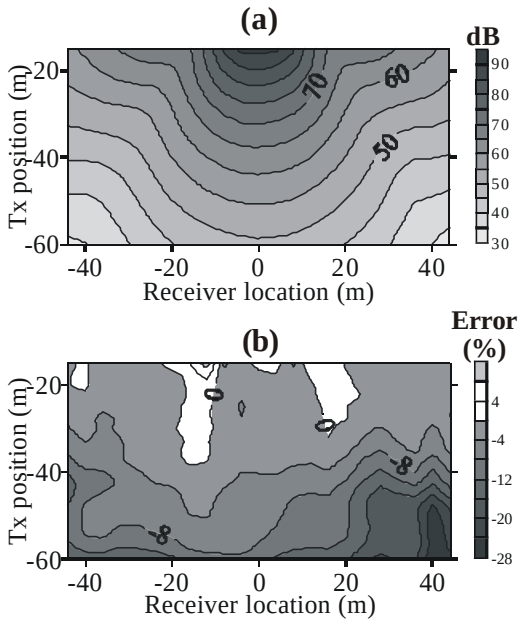

Tseng et al., Fig. 9, column width.

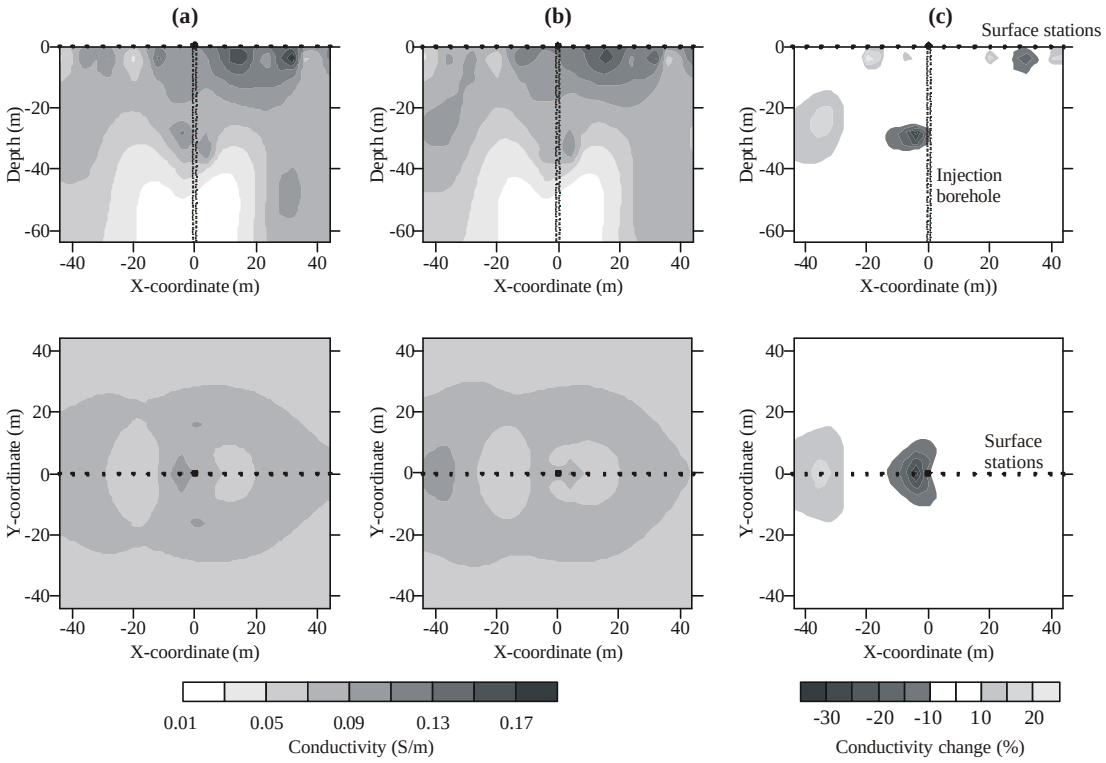

Tseng et al., Fig. 10, full page.